Progress In Electromagnetics Research B, Vol. 43, 129–150, 2012

ELECTROMAGNETIC RADIATION FROM UNBALANCED TRANSMISSION LINES

M. Miri* **and M. McLain**

Department of Electrical and Computer Engineering, UNC Charlotte, Charlotte, NC 28223, USA

Abstract—A theory for the electromagnetic radiation from unbalanced transmission lines is developed. It is shown that radiation results from the convection current that develops in unbalanced transmission lines where the resistances of the lines are unequal. The process that leads to the generation of the nonlinear convection current in unbalanced transmission lines is explained. It is proved that the classical transmission line theory is not valid for unbalanced lines. The convection current and the radiation forces are included in the transmission line equations to develop a generalized model valid for all two-conductor transmission lines. The generalized model is validated via comparisons of its numerical solutions with laboratory measurements.

1. INTRODUCTION

Radiated emissions from transmission lines have been known since the early 1900s [1] and they have been attributed to "common-mode currents" [2]. However, the mechanism that leads to the generation of these currents is not understood. The effect of a transmission line radiation on its propagation characteristic is observable in the laboratory as signal distortions in specific frequency ranges. Another observable phenomenon is that the propagation characteristic changes when objects, such as human hands, are moved around the transmission line, even around shielded coaxial cables [3]. This latter phenomenon is attributed to the equivalent transfer admittance of the cable [4]. The subject of this paper is the understanding of the mechanism that leads to radiation and nonlinear propagation characteristics in unbalanced transmission lines. Radiation from unbalanced structures is of great interest to the scientific community [5]

Received 6 September 2011, Accepted 20 August 2012, Scheduled 23 August 2012

* Corresponding author: Mehdi Miri (miri@uncc.edu).

and this paper furthers the understanding of this phenomenon. We will show that what is referred to as "common-mode current" in the literature is in fact convection current that arises in transmission lines with unequal conductor resistances. We will show that the flow of conduction currents in such lines give rise to unbalanced charge distributions and the flow of convection currents. Time-variation of the convection current results in electromagnetic radiation along the line. Convection current alters the propagation characteristic of the line in a complex way and causes nonlinearities that are not modeled by the classical transmission line theory. None of the generalizations of the classical theory found in the literature [6–12] model radiation or the flow of the nonlinear convection currents. Reference [13] models the quantum mechanical effect of discrete electronic charges in mesoscopic scale but does not consider the flow of bulk convection current or radiation. The theory presented in this paper is applicable in the evaluation and design of all two-conductor transmission lines.

2. CONVECTION CURRENTS IN UNBALANCED LINES

2.1. The Classical Theory and the Unbalanced Transmission Line

The classical transmission line theory has been developed based on the assumption that an incremental length of the line can be modeled by the equivalent circuit shown in Fig. 1. The transmission line equations based on this model are given by (1).

$$\frac{\partial v(t,z)}{\partial z} = -Ri(t,z) - L\frac{\partial i(t,z)}{\partial t} \tag{1a}$$

$$\frac{\partial i(t,z)}{\partial z} = -Gv(t,z) - C\frac{\partial v(t,z)}{\partial t} \tag{1b}$$

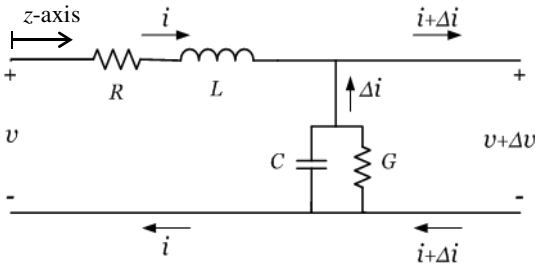

Figure 1. Classical incremental transmission line model.

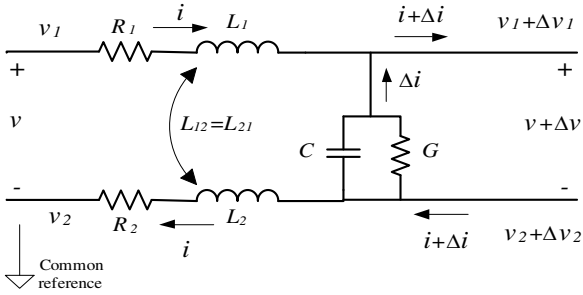

Figure 2. Unbalanced incremental transmission line model.

where $v(t,z)$ is the differential voltage between the two lines and $i(t,z)$ the conduction current in the two lines at time t and location z. The combined resistances and inductances of both lines per unit length (p.u.l.) are modeled by R and L. The p.u.l. capacitance between the two lines is modeled by C, and G is the p.u.l. conductance accounting for losses in the dielectric separating the two conductors. This model assumes that the transmission line is balanced and that the resistances and inductances of the two conductors can be lumped together. Let us examine these assumptions by rewriting (1) in terms of signals and parameters of each line as shown in Fig. 2

$$\frac{\partial v_1(t,z)}{\partial z} = -R_1 i(t,z) - L_1 \frac{\partial i(t,z)}{\partial t} - L_{12} \frac{\partial i(t,z)}{\partial t} \tag{2a}$$

$$\frac{\partial v_2(t,z)}{\partial z} = R_2 i(t,z) + L_2 \frac{\partial i(t,z)}{\partial t} + L_{21} \frac{\partial i(t,z)}{\partial t} \tag{2b}$$

$$\frac{\partial i(t,z)}{\partial z} = -G\left[v_1(t,z) - v_2(t,z)\right] - C \frac{\partial \left[v_1(t,z) - v_2(t,z)\right]}{\partial t} \tag{2c}$$

where $v_1(t,z)$ and $v_2(t,z)$ are the scalar voltages of the two conductors with respect to some common reference, and R_1 and R_2 are the two p.u.l. conductor resistances. $i(t,z)$ is assumed to be the same in each conductor for a given time and location as required by the classical theory. All the four inductive terms in (2) are derived from the Faraday's Law of Induction. The inductances L_1 and L_2 account for the p.u.l. voltages induced in each conductor by its own current. The inductances L_{12} and L_{21} account for the p.u.l. voltages induced in each conductor by the current in the other. The magnetic flux linking the transmission line circuit due to the current in one of the conductors induces an equal p.u.l. voltage in both conductors. This fact requires the equality of L_1 with L_{21} and the equality of L_2 with L_{12}. The magnetic flux linking the transmission line circuit due to the current

$i(t,z)$ in one of the conductors is equal to the magnetic flux linking the circuit due to the same current in the other conductor. Therefore, $L_1 = L_2$ and we can firmly conclude that all four inductances in (2) are equal and that each equals one-fourth of the total p.u.l. inductance of the transmission line L. The inductive voltage gradients on the right hand sides of (2a) and (2b) are magnetically induced and are equal along the two conductors. The resistive voltage gradients-$R_1 i$ and $R_2 i$ are due to nonzero charge gradients along the transmission line conductors. When $R_1 \neq R_2$, the charge distributions associated with the two resistively induced voltage gradients cannot totally balance each other via the shunt admittance and result in an unbalanced charge distribution along the conductor with higher resistance. For $R_1 > R_2$, the voltage gradient that is balanced along the two conductors is $\pm(R_2 i + 0.5L\frac{\partial i}{\partial t})$. The unbalanced component is obtained by adding (2a) to (2b). Letting $\partial v_u/\partial z \triangleq \partial v_1/\partial z + \partial v_2/\partial z$, this component is given by the classical theory as

$$\frac{\partial v_u(t,z)}{\partial z} = (R_2 - R_1)\, i\,(t,z) \tag{3}$$

This unbalanced voltage gradient develops along Conductor 1 that has higher resistance. The unbalanced charge distribution associated with the unbalanced voltage gradient does not contribute to the balanced charges on the shunt capacitance. Thus, the voltage across the transmission line's capacitance is not the same as the transmission line's differential voltage $v_1 - v_2$. This is a significant discovery and shows that the last term in (2c) is invalid, and that the classical transmission line theory is not applicable to unbalanced transmission lines.

2.2. The Convection Current

The unbalanced charges are free to interact with charges in the surrounding matter and with unbalanced charges at neighboring locations along Conductor 1. When the ratio of the transmission line's length (ℓ) to the wavelength (λ) is much smaller than unity, this interaction is mainly via stray capacitances with the surrounding matter. Otherwise, unbalanced charge distributions of both polarities develop along Conductor 1 and interact; giving rise to the convection current. The importance of this unbalanced convection current is that it leads to transverse electromagnetic radiation.

In any two-conductor transmission line, the balanced line charge density in C/m is given by

$$\rho_b(t,z) = cv(t,z) \tag{4}$$

where v is the voltage across the transmission line capacitance c. In an unbalanced transmission line with $R_1 > R_2$, the line charge density $\rho_2(t,z) = -\rho_b(t,z)$ and for the conductor with higher resistance, it is given by

$$\rho_1(t,z) = \rho_b(t,z) + \rho_u(t,z) \tag{5}$$

where ρ_u is the unbalanced line charge density in C/m. The unbalanced charge distribution is induced by the conduction current as shown by (3). The unbalanced charge density travels along the conductor as a transverse wave with a phase velocity equal to that of the conduction current. This wave motion does not result in convection of charges along the conductor. However, consider the distribution of unbalanced charges along Conductor 1 at time t as shown in Fig. 3. In this figure, the heights of the charge columns represent the magnitude and u_p denotes the phase velocity of the travelling $\rho_u(t,z)$. The convection velocities of the mth and the nth unbalanced electrons are denoted by u_m and u_n.

The life cycle of an unbalanced charge begins and ends when it is induced and then picked up by the flow of the conduction current. Assuming that $i(t,z)$ and $\rho_u(t,z)$ waves are travelling in the $+z$ direction, the leading edge of each charge packet is on the right of the packet. In metallic conductors, electrons are mobile and positively charged holes are stationary. In Fig. 3, subscript t denotes the trailing edge and subscript l denotes the leading edge of the unbalanced electron packets. Subscript m denotes the minima and subscript p denotes the maxima of the $\rho_u(t,z)$ wave. The locations z_{lB} and z_{rB} denote the transmission line's left and right boundaries. As the conduction current wave travels in the $+z$ direction, it picks up unbalanced electrons between z_t and z_m locations and deposits them between z_m and z_l locations, moving the unbalanced electron wave along with it. When an unbalanced electron is induced within the leading half of a negative packet, it experiences an acceleration in the $+z$ direction, according to the Coulomb's law, given by

$$a_n = \frac{e^2}{4\pi\epsilon m_e d_n^2} \tag{6}$$

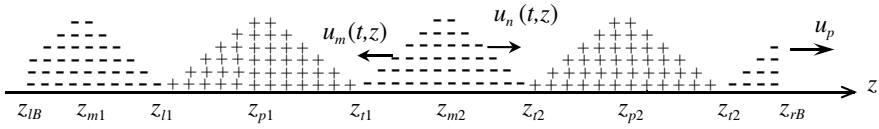

Figure 3. A travelling unbalanced charge distribution along an unbalanced transmission line.

where a_n is the acceleration of the nth electron, e the charge of an electron, m_e the mass of an electron, ϵ the effective permittivity of the medium, and d_n the distance between the nth electron and its counterpart hole within the leading positive packet. This acceleration gives rise to convection electron velocities and the convection current. As the distance between the nth electron and the leading positive packet increases with velocity $u_p - u_n$, it pairs with the closest positive hole that has not paired with a closer electron. That is, as the location of the nth electron shifts away from the leading edge of the negative charge packet, the location of its counterpart hole shifts away symmetrically from the trailing edge of the positive charge packet. Thus, the distance d_n increases with velocity $2(u_p - u_n)$. This distance varies from a minimum value in the order of the interatomic distance in the conductor's material to the maximum value of $\lambda/2$. Beyond the distance of $\lambda/2$, the electron becomes closer to the lagging positive packet and begins to decelerate and then accelerate in the opposite direction. The electron is now in the trailing half of its packet and the distance d_n begins to decrease at the rate of $2(u_p + u_n)$. The variation in the convection velocities of the unbalanced electrons leads to electromagnetic radiation.Radiation forces oppose the Coulomb forces on the convection electrons and the acceleration in (6) is impeded. The unbalanced charges are part of the conduction process and the flow of convection current distorts the conduction current. The unbalanced electrons induced between z_m and z_l locations experience different accelerations and attain convection velocities that depend on the locations where they are induced. Let t_0 denote the time and z denote the location within the leading half of the negative packet where the group n of the unbalanced electrons are induced, then $d_n = 2(z_l(t) - z)$. Noting that $u_p \gg u_n$, the distance d_n increases at the rate of about $2u_p$ and can be defined by $d_n = 2[z_l(t_0) + (t - t_0)u_p - z]$. The unimpeded velocity of this group of electrons for $t_0 < t < t_{\lambda/4}$ can be determined from integration of (6)

$$\begin{aligned} u_n(t,z) &= \int_{t_0}^{t} \frac{e^2 dt}{16\pi\epsilon m_e [z_l(t_0) + (t - t_0)u_p - z]^2} \\ &= \xi \left[\frac{1}{z_l(t_0) - z} - \frac{1}{z_l(t) - z} \right] \end{aligned} \tag{7}$$

where $\xi \triangleq \frac{e^2}{16\pi\epsilon m_e u_p}$ and $t_{\lambda/4} = t_0 + \frac{1}{u_p}[\frac{\lambda}{4} + z - z_l(t_0)]$ is the time beyond which the group n electrons experience accelerations in the opposite direction. Within the leading half of a negative packet, the unbalanced electrons that are induced at the leading edge within the interatomic distance from the trailing edge of the leading positive packet attain

the maximum possible velocity because they experience the strongest Coulomb forces. This maximum velocity is in the $+z$ direction, does not depend on t_0, and is approximated by

$$u_{\max} = \int_0^{t_{\max}} \frac{e^2 dt}{16\pi\epsilon m_e [d_a + u_p t]^2} = \xi \left[\frac{1}{d_a} - \frac{1}{d_a + u_p t_{\max}} \right] \quad (8)$$

where d_a is the interatomic distance in the conductor material, $t_{\max} = \frac{1}{u_p}[\frac{\lambda}{4} - 2d_a]$, and $\frac{\lambda}{4} - 2d_a$ is the length of the region within the leading half of the negative packet where unbalanced electrons experience Coulomb acceleration. Note that $u_{\max}$ becomes negligible for wavelengths in the order of d_a. To confirm our assumption that $u_p \gg u_n$, we evaluate (8) for copper with $d_a \approx 256\,\text{pm}$, $\epsilon = \epsilon_0$, and $u_p = 2 \times 10^8\,\text{m/s}$. For frequencies less than $10^{16}\,\text{Hz}$, (8) evaluates to $u_{\max} \approx 1230\,\text{m/s}$.

The convection current $i_c(t, z)$ can be defined, using the average velocity of the unbalanced electrons $u_a(t, z)$, by

$$i_c(t, z) = \rho_u(t, z) u_a(t, z); \quad \rho_u < 0 \quad (9)$$

The unbalanced electrons that contribute to the average velocity at (t, z) are those that are induced at z between the time t_n and t, where t_n is the time when the leading edge of the unbalanced electron wave is at $z + d_a$. Thus, the average velocity of the unbalanced electrons at any location within the leading half of a negative packet can be determined from the weighted average of $u_n(t, z)$ over the range $z + d_a \le z_l(t_0) \le z_l(t)$ with $t_n \le t_0 \le t$, that is

$$u_a(t, z) = \frac{\int_{z+d_a}^{z_l(t)} u_n(t, z) \rho_u(t_0, z) dz_l(t_0)}{\int_{z+d_a}^{z_l(t)} \rho_u(t_0, z)\, dz_l(t_0)} \quad (10)$$

where the variable of integration is the location of the leading edge of the unbalanced electron wave at the time t_0 when each group of electrons with density $\rho_u(t_0, z)$ is induced at time t_0 and location z. In order to evaluate (10), we make the simplifying assumption that the charge densities of the newly induced electrons at location z over the time $t_n \le t_0 \le t$ are the same and independent from $z_l(t_0)$. This assumption estimates the spatial distribution of $\rho_u(t, z)$ with a triangular waveform in the evaluation of (10). It results in the cancellation of $\rho_u(t_0, z)$ from the numerator and the denominator of (10) which then, using (7), reduces to

$$\begin{aligned} u_a(t, z) &= \frac{\xi}{z_l(t) - z - d_a} \int_{z+d_a}^{z_l(t)} \left[\frac{1}{z_l(t_0) - z} - \frac{1}{z_l(t) - z} \right] dz_l(t_0) \\ &= \frac{\xi}{z_l(t) - z - d_a} \ln \frac{z_l(t) - z}{d_a} - \frac{\xi}{z_l(t) - z} \end{aligned} \quad (11)$$

where $2d_a \leq z_l(t) - z \leq \lambda/4$. Eq. (11) is valid for any location within the leading half except that at locations d_a from the leading edge of the $\rho_u(t, z)$ wave, the unbalanced electrons will always have zero velocity.

To determine the convection current using (9), we also need to determine the average velocity of the unbalanced electrons at any location within the trailing half of a negative packet. All unbalanced electrons are induced within the leading half and as the $\rho_u(t, z)$ wave travels in the $+z$ direction, they become part of the trailing half with initial velocities in the $+z$ direction while experiencing accelerations in the $-z$ direction. Similarly, the average velocity of the unbalanced electrons at any location within the trailing half of a negative packet can be shown to be

$$u_a(t, z) = \xi \left[\frac{4}{\lambda - 4d_a} \ln \frac{\lambda}{4d_a} - \frac{1}{z - z_t(t)} \right] \tag{12}$$

where $z_t(t)$ is the trailing edge of the unbalanced electron packet and $d_a \leq z - z_t(t) \leq \lambda/4$. Note that at locations d_a from the trailing edge of the $\rho_u(t, z)$ wave, the unbalanced electrons attain their highest velocity in $-z$ direction.

Equations (9), (11) and (12) can be used to determine the convection current at the interior locations along the line. Near the boundaries, the unbalanced electrons may have no counterpart holes and may not experience any acceleration. For example, at the left boundary in Fig. 3, the unbalanced electrons between z_{lB} and z_{m1} have no counterpart holes and do not experience acceleration in the $-z$ direction. These electrons maintain the initial velocities they attain in the $+z$ direction when they are at the peak of the negative packet nearest the left boundary. The boundary conditions are time-varying and, at times, apply to regions near the boundaries rather than to single locations. The boundary conditions are formulated in Section 3 where we develop the unbalanced transmission line model.

3. THE UNBALANCED TRANSMISSION LINE MODEL

The conduction current at any location along a conductor is defined as the time-rate of the longitudinal flow of conduction electrons at that location. For the same conduction current to flow in both conductors of an unbalanced transmission line, a greater line charge density develops along the conductor with higher resistance. The algebraic sum of the charge densities along the two conductors is the unbalanced charge density that exists along the conductor with higher resistance. As discussed in the previous section, this unbalanced charge distribution gives rise to the convection current. The convection current is internal

to the transmission line and is discontinuous at boundaries with lump parameter loads and sources. The boundary conditions for the conduction current are forced by the external source voltage and load impedance. The convection flow of the unbalanced electrons leads to electromagnetic radiation and to impeding radiation forces that must be accounted for. It is customary to use series radiation resistance (R_r) and inductance (L_r) to model the radiation forces. We will account for radiation forces directly.

Consider the two-conductor unbalanced transmission line shown in Fig. 4 where it is assumed that the transmission line conductors are of length ℓ and are in parallel with the z-axis.

In Fig. 4, $i(t,z)$ is the conduction current, $i_c(t,z)$ is the convection current, and $v(t,z)$ is the scalar potential across the transmission line's capacitance. Assuming that Conductor 1 has a higher resistance than Conductor 2, an unbalanced charge distribution, $\rho_u(t,z)$, develops along Conductor 1 (similar to Fig. 3). This unbalanced charge distribution can be related to the longitudinal component of its electric field via the point form of Gauss' law

$$\boldsymbol{\nabla}\cdot\mathbf{D}(t,z) = \frac{\partial D_u}{\partial z} = \epsilon\frac{\partial E_u}{\partial z} = \frac{1}{S}\rho_u(t,z) \tag{13}$$

where D_u is the z-component of the electric flux density $\mathbf{D}$ resulting from ρ_u, $\boldsymbol{\nabla}\cdot$ the divergence operator, E_u the z-component of the electric field intensity resulting from the unbalanced charge distribution, ϵ the effective permittivity of the medium, and S the cross-sectional area of the conductor. Eq. (13) relates the unbalanced charge distribution to its own electric field intensity. This electric field intensity is related to the unbalanced voltage gradient via $\mathbf{E_u} = -\boldsymbol{\nabla}v_u$ or

$$E_u(t,z) = -\frac{\partial v_u(t,z)}{\partial z} \tag{14}$$

Note that E_u represents the electric field of the unbalanced charges and that the time-derivative of the vector magnetic potential, the $-\partial\mathbf{A}/\partial t$ term, is zero. Plugging (14) in (13), solving for $\rho_u(t,z)$ and using (3),

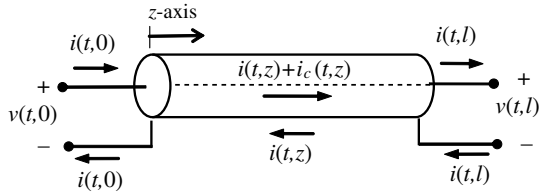

Figure 4. An unbalanced transmission line with $R_1 > R_2$.

we get

$$\rho_u(t,z) = -C_v \frac{\partial^2 v_u}{\partial z^2} = C_v \left(R_1 - R_2\right) \frac{\partial i(t,z)}{\partial z} \tag{15}$$

where $C_v \triangleq \epsilon S$ is the volume capacitance in $F - m$.

We can now solve for the convection current by combining (9), (11), (12), and (15)

$$i_c(t,z) = \begin{cases} \left[\frac{\xi}{z_l(t)-z-d_a} \ln\left(\frac{z_l(t)-z}{d_a}\right) - \frac{\xi}{z_l(t)-z}\right]\left[C_v(R_1-R_2)\frac{\partial i(t,z)}{\partial z}\right]; \\ \qquad\qquad \rho_u(t,z) < 0 \quad \text{and} \quad 2d_a \le z_l(t) - z \le \lambda/4 \\ \left[\frac{4\xi}{\lambda-4d_a} \ln\left(\frac{\lambda}{4d_a}\right) - \frac{\xi}{z-z_t(t)}\right]\left[C_v(R_1-R_2)\frac{\partial i(t,z)}{\partial z}\right]; \\ \qquad\qquad \rho_u(t,z) < 0 \quad \text{and} \quad d_a \le z - z_t(t) \le \lambda/4 \\ 0; \qquad\qquad \rho_u(t,z) \ge 0 \end{cases} \tag{16}$$

This is the so-called common-mode current, and it is the source of electromagnetic radiation. Time-variation of the unbalanced electrons' convection velocities given by (11) and (12) results in radiation forces that impede the Coulomb accelerations defined by (6). The magnitude of the radiation force on a convection electron is proportional to the electron's acceleration. As the potential energy of the unbalanced charge distribution is converted to the kinetic energy in the motion of the unbalanced electrons, additional potential energy is spent to overcome the opposing radiation forces. The convection electrons attain velocities that are lower than those defined by (11) and (12), which are valid only in the absence of radiation. We account for radiation forces by redefining the acceleration in (6) as

$$a_n = \frac{e^2}{4\pi\epsilon(m_e+m_r)d_n^2} \tag{17}$$

where m_r is the proportionality constant in modeling the radiation force as $m_r a_n$. With this definition, all previous equations remain valid with the constant ξ redefined as

$$\xi \triangleq \frac{e^2}{16\pi\epsilon(m_e+m_r)u_p} \tag{18}$$

The convection flow of the unbalanced electrons distorts the conduction current wave shape. Referring to Fig. 3, the travelling conduction current wave induces unbalanced electrons within the leading halves of the negative packets between locations z_m and z_l. These electrons gain convection velocities and rejoin the conduction electrons in the trailing halves between z_t and z_m locations. That is, when the unbalanced electrons join the conduction current, they

have initial velocities that give rise to additional conduction current, distorting its waveshape. To model the contribution of the convection flow of the unbalanced electrons to the conduction current, the time-rate at which these electrons interact with the conduction electrons should be determined. We note that (9) yields

$$\frac{\partial i_c(t,z)}{\partial t} = u_a(t,z)\frac{\partial \rho_u(t,z)}{\partial t} + \rho_u(t,z)\frac{\partial u_a(t,z)}{\partial t} \tag{19}$$

The first term in (19) is the time-rate of conversion of the convection current to conduction current and is responsible for the distortion of the conduction current. Within the trailing-half of the unbalanced electron packet, where $\frac{\partial \rho_u}{\partial t} > 0$, this conversion rate is positive. Within the leading-half, where $\frac{\partial \rho_u}{\partial t} < 0$, the conversion rate is negative. This term needs to be included in the unbalanced transmission line equation for the conduction current. The second term in (19) is due to time-variation of the convection velocity and, along with the first term, is responsible for electromagnetic radiation. The convection current $i_c(t,z)$ is used in Section 6 to determine the patterns of radiation from unbalanced transmission lines.

We now substitute (15) in the first term in (19) and include this term in the conduction current equation to obtain the unbalanced transmission line equations:

$$\frac{\partial i(t,z)}{\partial t} + C_v(R_1 - R_2)u_a(t,z)\frac{\partial^2 i(t,z)}{\partial t \partial z} = -\frac{1}{L}\left[Ri(t,z) + \frac{\partial v(t,z)}{\partial z}\right]; \quad \frac{\partial \rho_u}{\partial t} \geq 0 \tag{20a}$$

$$\frac{\partial i(t,z)}{\partial t} - C_v(R_1 - R_2)u_a(t,z)\frac{\partial^2 i(t,z)}{\partial t \partial z} = -\frac{1}{L}\left[Ri(t,z) + \frac{\partial v(t,z)}{\partial z}\right]; \quad \frac{\partial \rho_u}{\partial t} \leq 0 \tag{20b}$$

$$\frac{\partial v(t,z)}{\partial t} = -\frac{1}{C}\left[Gv(t,z) + \frac{\partial i(t,z)}{\partial z}\right] \tag{20c}$$

$$u_a(t,z) = \begin{cases} \frac{\xi}{z_l(t)-z-d_a}\ln\frac{z_l(t)-z}{d_a} - \frac{\xi}{z_l(t)-z}; \\ \rho_u(t,z) < 0 \quad \text{and} \quad 2d_a \leq z_l(t) - z \leq \lambda/4 \\ \xi\left[\frac{4}{\lambda - 4d_a}\ln\frac{\lambda}{4d_a} - \frac{1}{z - z_t(t)}\right]; \\ \rho_u(t,z) < 0 \quad \text{and} \quad d_a \leq z - z_t(t) \leq \lambda/4 \\ 0; \qquad\qquad \rho_u(t,z) \geq 0 \end{cases} \tag{20d}$$

The boundary conditions for $u_a(t,z)$ are nonstandard as explained in the last paragraph of Section 2. Referring to Fig. 3, we note that

when the trailing-half of a negative packet is at the load boundary (right boundary in Fig. 3), the second equation in (20d) applies. When the leading-half of a negative packet is at the source boundary, the first equation in (20d) applies. However, the velocity equations for the trailing-half electrons near the source boundary and for the leading-half electrons near the load boundary are different from (20d). The boundary conditions are determined using integral equations similar to (11) but with integration limits applicable to the boundaries.

For the source boundary at $z = 0$, the boundary condition for the conduction current and the differential voltage is

$$v\,(t,0) = v_s(t) - \; R_s i\,(t,0) \tag{21a}$$

For the convection velocity of the unbalanced electrons near the source boundary, the boundary condition is defined either by (20d) or, for the trailing-half electrons, by

$$u_a(t,z) = \begin{cases} \xi\left[\frac{2}{z} - \frac{1}{z-z_{t1}(t)} + \frac{4}{\lambda-4d_a}\ln\frac{\lambda}{4d_a} - \frac{4}{\lambda}\right]; \\ \rho_u(t,z) < 0, \quad 2d_a \le z \le 2z_{t1}(t) \text{ and } d_a \le z_{t1}(t) \le \lambda/4 \\ \xi\left[\frac{4}{\lambda-4d_a}\ln\frac{\lambda}{4d_a} - \frac{4}{\lambda}\right]; \\ \rho_u(t,z) < 0 \text{ and } z < z_{m1}(t) < \lambda/4 \;\text{ or }\; 2z_{t1}(t) < z < z_{m1}(t) \end{cases} \tag{21b}$$

In (21a), $v_s(t)$ is the source voltage and R_s the source internal resistance. In (21b), z_{t1} and z_{m1} are as defined in Fig. 3. For regions near the source boundary not defined in (21b), equations in (20d) apply.

For the load boundary at $z = l$, the boundary condition for the conduction current and the differential voltage is

$$v\,(t,\ell) = R_L i\,(t,\ell) \tag{22a}$$

where R_L is the load resistance. For the convection velocity of the unbalanced electrons near the load boundary, the boundary condition is defined either by (20d) or, for the leading-half electrons, by

$$u_a(t,z) = \frac{\xi}{z_{mk}\,(t) - z + \lambda/4 - d_a}\left[\ln\left(\frac{\ell - z}{2d_a}\right) - 1 + \frac{2d_a}{\ell - z}\right]; \qquad \rho_u(t,z) < 0 \quad \text{and} \quad z_{mk}(t) \le z \le \ell - 2d_a \tag{22b}$$

where $z_{mk}(t)$ is the negative peak of $\rho_u(t,z)$ closest to the load boundary.

Equations (20), (21), and (22) can be used to model any two-conductor unbalanced transmission line. For balanced lines, $R_1 = R_2$, $\rho_u = i_c = 0$, and the unbalanced equations reduce to the two classical equations in (1) with the same frequency-domain definitions

for the propagation constant and the characteristic impedance. Also, in transmission lines with low degree of unbalancedness where R_1 and R_2 are not equal but are close, one may neglect radiation and use the classical model. However, to determine the convection current and to analyze the emitted radiation, the nonlinear system of equations in (20)–(22) need to be solved in time-domain. In Section 5, the Finite-Difference Time-Domain (FDTD) method [14–16] is used to solve these equations for an unbalanced transmission line consisting of copper and nickel-titanium lines. The FDTD solutions of the unbalanced model and of the classical model equations are then compared with experimental results.

4. EXPERIMENTAL RESULTS

The theory of radiation from unbalanced lines presented in Section 2 led to the derivation of the model presented in Section 3. To validate the presented theory and to develop a trust in the model, laboratory tests have been conducted. Fig. 5 shows the experimental set up where balanced and unbalanced transmission lines (T2) have been tested. The transmission line T1 represents the coaxial leads of the function generator used with signal $v_s(t)$ and internal resistance R_s. L_{ss} and L_{sr} represent the inductances of the coax's signal and reference terminations that connect to the sending end of T2. The load resistance at the receiving end of T2 is represented by R_L. The circuitry to the right of R_L models the probe and the channel input impedance of the battery-powered 200 MHz oscilloscope used. The probe's coax represented by T3 is itself an unbalance transmission line with its center conductor being a highly resistive Nichrome wire which is commonly used in high end scopes to damp out ringing.

Convection current along an unbalanced T2 cannot be measured directly and the objective of our experiments was to capture the distortion of the conduction current caused by the convection current. To ensure that any distortion observed in the conduction current is

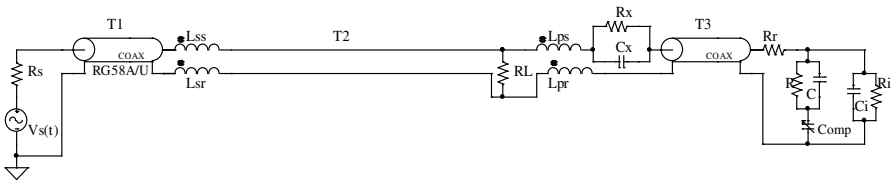

Figure 5. Experimental set up for the validation of the unbalanced transmission line theory.

only the result of the flow of convection electrons, we first verified that no distortion is observed when the transmission line T2 is balanced. This verification is important particularly because the scope's probe coax is a potential source of radiation and distortion. The arrangement shown in Fig. 5 was set up inside a shielded room where all tests were conducted. The shielded room was used to minimize interference and possible distortions from external sources.

Balanced tests were conducted with two identical conductors used to construct T2 as a transmission line with parallel conductors. In one test, T2 was constructed from two identical solid bare copper wires.In the second test, T2 was constructed from two identical solid Nickel-Titanium (Nitinol) wires. The unbalanced test was conducted with one copper wire and one Nitinol wire to construct T2 as an unbalanced transmission line.To minimize the interaction of T2 with its surrounding matter, the sending and receiving ends of T2 were mounted on the two sides of a ⊔-shape all wood structure with a 1.8 m base. The two parallel lines of T2 were stretched in air at the height of 1.35 m, providing more than 1m clearance all around. A 50 Ω source with a matched coax, a resistive load of 10 Ω, and a scope probe setting of ×10 was used in all experiments. The low resistance load was used to maximize the conduction current and to eliminate scope probe distortions that can occur with high impedance loads. The transmission line data for T2 used in the three experiments are given in Table 1. The parameter values shown are the measured values with the theoretical values for parallel two-wire transmission lines shown in parentheses. Dielectric losses are assumed to be negligible.

In all three experiments, the source voltage was sinusoidal and its frequency was varied from 1 MHz to 100 MHz, and the conduction current was observed via the load voltage on the scope.

Table 1. Data for the three tested transmission lines.

	Experiment 1		Experiment 2		Experiment 3	
	Balanced Copper Lines		Balanced Nitinol Lines		Unbalanced Copper/Nitinol Lines	
	Conductor 1	Conductor 2	Conductor 1	Conductor 2	Conductor 1	Conductor 2
Conductor Material	solid copper	solid copper	solid Nitinol	solid Nitinol	solid Nitinol	solid copper
Conductordia (mm)	0.644	0.644	0.202	0.202	0.202	0.644
R1(Ω/m)	0.069 (0.053)	-	29.4 (27.8)	-	29.4 (27.8)	-
R2(Ω/m)	-	0.069 (0.053)	-	29.4 (27.8)	-	0.069 (0.053)
L (μH/m)	0.711 (0.72)		1.1 (1.19)		0.957	
C (pF/m)	16.3 (15.5)		10.5 (9.3)		13.6	
Line Length(m)	1.81	1.81	1.81	1.81	1.81	1.81
Line Separation (mm)	2		2		2	

In Experiment 1, where the line's total resistance was in milli-Ohms, the source voltage amplitude was 5 V whereas in Experiments 2 and 3, the amplitude was 10 V. In Experiments 1 and 2, no distortion of the conduction current was observed at any frequency. In Experiment 3, distortions of the conduction current was observed at specific frequencies. Fig. 6 shows the typical distortion of the load voltage waveforms observed in the lab.

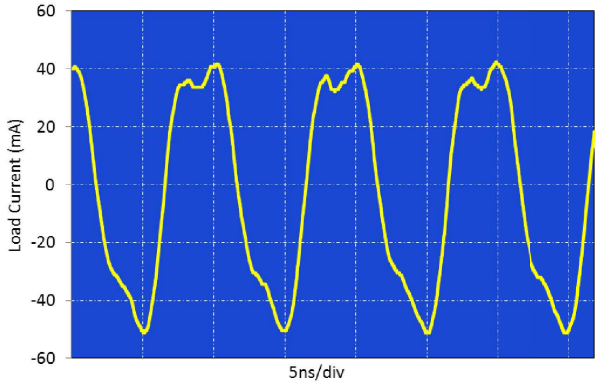

Figure 6. Copper/Nitinol transmission line's load current distortion observed in the lab.

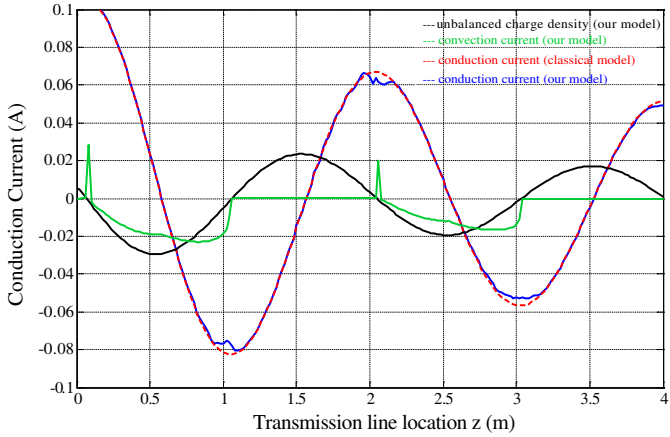

Figure 7. Conduction current, convection current and unbalanced charge density along the Copper/Nitinol line.

5. COMPUTER SIMULATIONS AND MODEL VALIDATION

The FDTD solution of the unbalanced transmission line model described by (20)–(22) can be shown to be

$$\begin{aligned}
i(t+\Delta t,z) &= \frac{1}{1-b_1u_a(t,z)}\{[b_1u_a(t,z)+b_2]\,i(t,z)+b_1u_a(t,z)\\
&\quad [i(t+\Delta t,z-\Delta z)-i(t,z-\Delta z)]\\
&\quad +b_3[v(t,z)-v\,(t,z+\Delta z)]\}\\
v\,(t+\Delta t,z) &= b_4v(t,z)+b_5\,[i\,(t,z-\Delta z)-i(t,z)]\\
v\,(t+\Delta t,0) &= v_s\,(t+\Delta t)-\ R_si\,(t+\Delta t,0)\\
i\,(t+\Delta t,l) &= \frac{1}{R_L}v\,(t+\Delta t,l)\\
v\,(0,0) &= 0.5v_s\,(0)\\
i\,(0,0) &= \frac{0.5}{R_s}v_{\ s}\ (0)\\
\rho_u(t,z) &= \frac{C_v\,(R_1-R_2)}{\Delta z}\,[i\,(t,z)-i\,(t,z-\Delta z)]
\end{aligned} \tag{23}$$

In (23), $b_1 = \frac{C_v(R_1-R_2)}{\Delta z}$ where $\frac{\partial\rho_u}{\partial t} < 0$ and $b_1 = -\frac{C_v(R_1-R_2)}{\Delta z}$ where $\frac{\partial\rho_u}{\partial t} > 0$, $b_2 = 1-\frac{R\Delta t}{L}$, $b_3 = \frac{\Delta t}{L\Delta z}$, $b_4 = 1-\frac{G\Delta t}{C}$, $b_5 = \frac{\Delta t}{C\Delta z}$, a mesh size of $\Delta z \times \Delta t$ has been assumed, and all initial conditions not specified are zero.

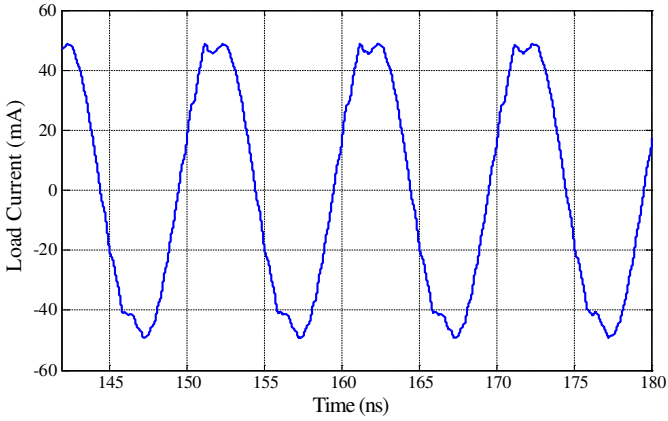

Figure 8. Copper/Nitinol transmission line's load current from model simulation.

At every grid point (t, z), $\rho_u(t, z)$ is used to determine the distances $z_l(t) - z$ and $z - z_t(t)$ which are then used to calculate $u_a(t, z)$. For the interior grid points, $u_a(t, z)$ is determined from (20d), for the source boundary points, it is determined from (21b), and for the load boundary points, it is determined from (22b).

These FDTD equations are solved for the unbalanced transmission line described in Table 1 using the parameters shown. Fig. 7 shows the simulated spatial distributions of the convection current, the conduction current, and the unbalanced charge distribution along the copper-Nitinol transmission line. The conduction current solution of the classical transmission line equations is shown for comparison. Only the conduction currents are plotted to scale.

Figure 8 shows the simulated steady state conduction current at the load for this unbalanced transmission line. The simulated load current shows distortions similar to those measured in the lab as shown in Fig. 6. The distortions are mainly near the peaks of the conduction current waveform because these locations correspond to the $+/-$ unbalanced charge packets' boundary locations where the convection current is highest as seen in Fig. 7. The asymmetrical distortions of the conduction current are caused by the flow of the asymmetrical convection current.

6. THE RADIATION PATTERNS

The travelling wave nature of the convection current results in radiation patterns that are intrinsically bipolarized and time-variant. Assuming an unbalanced transmission line of length ℓ along the z-axis, the retarded vector magnetic potential $\mathbf{A}$ has only a z-component given by

$$A_z = \frac{\mu_0}{4\pi}\left[\int_0^{\ell} \frac{i_c(t - \frac{R}{c}, z')}{R} dz'\right] \tag{24}$$

where i_c is the convection current given by (16), and z' denotes the source location along the z-axis. μ_0 is the permeability of free space, $t - R/c$ the retarded time, R the magnitude of the position vector locating the field point relative to the source point, and c the speed of light in free space. In spherical coordinates (r, θ, φ), $\mathbf{A}$ has A_r and A_θ components but only the A_θ component contributes to the far field radiation. The magnetic component of the radiation in the far field is

$$\mathbf{H} = H_\varphi \mathbf{a}_\varphi = \frac{1}{\mu_0}\boldsymbol{\nabla} \times \mathbf{A} = \frac{-\sin(\theta)}{\mu_0}\frac{\partial A_z}{\partial r}\mathbf{a}_\varphi \tag{25}$$

where $\boldsymbol{\nabla}\times$ is the curl operator, $\mathbf{a}_\varphi$ the unit vector in the φ direction, and A_z given by (24). Whereas the radiating current in a conventional

antenna is a standing wave, i_c in (24) is a travelling wave.We express the nonlinear convection current as a travelling wave using the Discrete Fourier Transform (DFT) approximation for its spatial distribution given by

$$i_c(t,z') \approx \sum_{k=1}^{N-1} \left\{ a_k \cos \mathrm{k}\left(\frac{2\pi z'}{\lambda_c} - 2\omega t \right) + b_k \sin \mathrm{k}\left(\frac{2\pi z'}{\lambda_c} - 2\omega t \right) \right\} \quad (26)$$

where a_k and b_k are the DFT coefficients, $\lambda_c = \lambda/2$. λ is the conduction current's wavelength, ω the source frequency, and 2ω the fundamental frequency of i_c used in its DFT approximation. To obtain the corresponding radiation pattern, we plug (26) in (24) and (24) in (25). Making the common assumptions that $R = r$ in the denominator and $R = r - z' \cos\theta$ in the numerator, the magnetic component of the

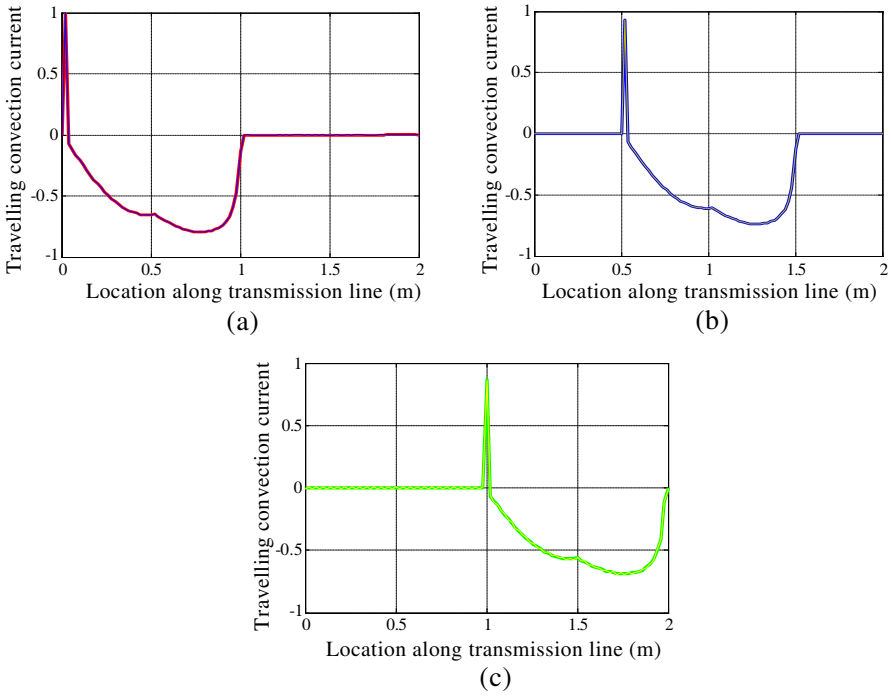

Figure 9. (a) Convection current and its DFT approximation. (b) Convection current and its DFT approximation. (c) Convection current and its DFT approximation.

far field radiation becomes

$$H_\varphi(r,\theta,t)\approx\frac{-\beta_s\sin\theta}{4\pi r(\beta-\beta_s cos\theta)}\sum_{k=1}^{N-1}\{a_k\cos\left[2k\left((\beta-\beta_s\cos\theta)z'+\beta_s r-\omega t\right)\right]$$
$$+b_k\sin\left[2k\left((\beta-\beta_s\cos\theta)z'+\beta_s r-\omega t\right)\right]\}_{z=z_1'}^{z_2'} \quad (27)$$

where the phase constants $\beta = 2\pi/\lambda$ and $\beta_s = 2\pi/\lambda_s$ with $\lambda_s = c/f$ being the radiation wavelength in space. The integration limits in (24) have been replaced by z_1' and z_2' that define the regions of nonzero convection current along the transmission line.

Figures 9(a)–9(c) show the snapshots of the convection current distribution at times $t_1 < t_2 < t_3$ as it travels along the copper/Nitinol transmission line of one wavelength long. Also shown in these figures are the DFT approximations (with $N = 50$) that are used to evaluate (27); DFT approximations are indistinguishable from the

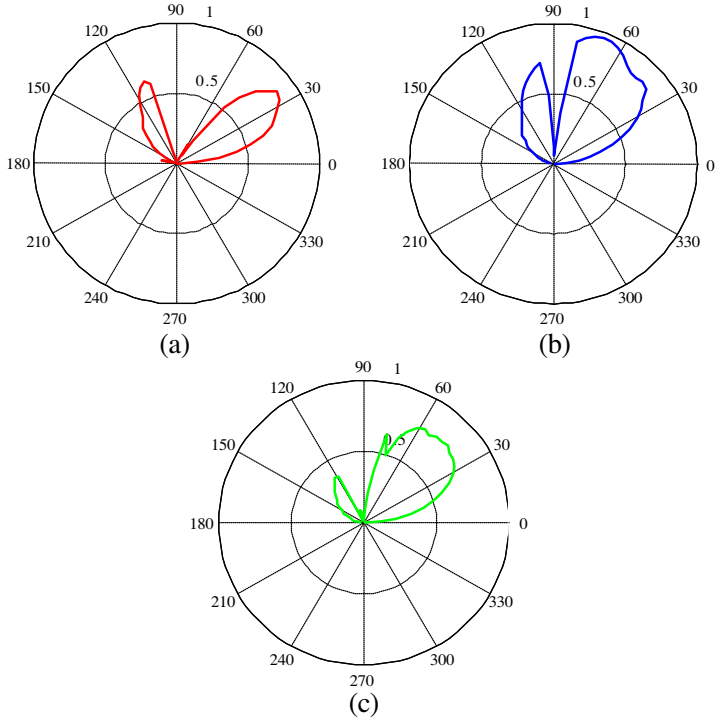

Figure 10. (a) Radiation pattern for the current in Fig. 9(a). (b) Radiation pattern for the current in Fig. 9(b). (c) Radiation pattern for the current in Fig. 9(c).

actual convection currents. With the source frequency of 100 MHz and the conduction current's phase velocity of $u_p = 2 \times 10^8$ m/s, we have a wavelength of $\lambda = 2$ m. To determine the radiation patterns for these current distributions, we let $t_1 = 0$, find $t_2 = 0.5/u_p = 2.5$ ns and $t_3 = 1/u_p = 5$ ns, and evaluate (27) with $z_1' = 0$, $z_2' = 1$ (Fig. 10(a)), $z_1' = 0.5$, $z_2' = 1.5$ (Fig. 10(b)), and $z_1' = 1, z_2' = 2$ (Fig. 10(c)). The normalized E-plane radiation patterns shown in Figs. 10(a)–10(c) are evaluated with $r = 100$ m and are plotted for $0 \leq \theta \leq \pi$.

7. CONCLUSION

For about a century, transmission line radiation has been attributed to the mysterious "common-mode current" without knowing its nature or the process that gives rise to its generation. We have shown that transmission line radiation is due to the time-variation of the convection currents that develop along unbalanced lines. We have developed a theory for the generation of this convection current. This theory enabled us to develop a transmission line model that can be used in the analysis and understanding of the nonlinear behaviors of unbalanced transmission lines observed in the field. We have verified this model via computer simulations and laboratory tests.

The spatial distribution of the convection current in an unbalanced transmission line is more controllable than the radiating current in a conventional antenna. The theory we have presented can be expanded to help design travelling wave narrow-beam antenna systems. This work is currently under investigation.

ACKNOWLEDGMENT

Mr. Jason Ryan McCall, an undergraduate student in our B.S.E.E. program, was instrumental in the construction and testing of the three transmission lines described in Table 1. It was a pleasure to work with Ryan for his work ethics, motivation, and exceptional attitude toward learning. We would like to thank the UNC Charlotte's Office of Academic Affairs for its "Charlotte Research Scholars" program that made Ryan's participation possible through financial support.

REFERENCES

1. Manneback, C., "Radiation from transmission lines," *AIEE Transactions,* Vol. XLII, 289–301, 1923.

2. Moongilan, D., "Radiation characteristics of short unterminated transmission lines," *IEEE International Symposium on Electromagnetic Compatibility*, 57–62, 2009.
3. Morishita, H., H. Furuuchi, and K. Fujimoto, "Performance of balance-fed antenna system for handsets in the vicinity of a human head or hand," *IEE Proc. Microwaves, Antennas Propagation,* Vol. 149, No. 2, 85–91, Apr. 2002.
4. Haase, H. and J. Nitsch, "High frequency model for the transfer impedance based on a generalized transmission-line theory," *IEEE International Symposium on Electromagnetic Compatibility*, Vol. 2, 1242–1247, 2001.
5. Yang, N., C. Caloz, and K. Wu, "Greater than the sum of its parts," *IEEE Microwave Magazine*, 69–82, Jun. 2010.
6. Haase, H., T. Steinmetz, and J. Nitsch, "New propagation models for electromagnetic waves along uniform and nonuniform cables," *IEEE Transactions on Electromagnetic Compatibility*, Vol. 46, No. 3, 345–352, 2004.
7. Tang, M. and J. F. Mao, "Transient analysis of lossy nonuniform transmission lines using a time-step integration method," *Progress In Electromagnetics Research*, Vol. 69, 257–266, 2007.
8. Khalaj-Amirhosseini, M., "Analysis of coupled or single nonuniform transmission lines using step-by-step numerical integration," *Progress In Electromagnetics Research*, Vol. 58, 187–198, 2006.
9. Bhattacharyya, A. K., L. Shafai, and R. Gary, "Microstrip antenna — A generalized transmission line," *Progress In Electromagnetics Research*, Vol. 4, 45–84, 1991.
10. Maffucci, A., G. Miano, and F. Villone, "An enhanced transmission line model for conducting wires," *IEEE Transactions on Electromagnetic Compatibility,* Vol. 46, No. 4, 512–528, 2004.
11. Wendt, D. O. and J. L. Ter Haseborg, "Consideration and representation of radiation losses in the transmission line theory," *IEEE Antennas and Propagation Society International Symposium,* Vol. 3, 1948–1951, 1994.
12. Kami, Y. and R Sato, "Analysis of radiation characteristics of a finite-length transmission line using a circuit-concept approach," *IEEE Transactions on E lectromagnetic Compatibility*, Vol. 30, No. 2, 114–121, 1988.
13. Chandia Valenzuela, K. J. and J. C. Flores, "Mesoscopic dual transmission line with discrete charge," *Journal of Electromagnetic Waves and Applications,* Vol. 23, Nos. 8–9, 1021–1028, 2009.

14. Zhang, Y.-Q. and D.-B. Ge, "A unified FDTD approach for electromagnetic analysis of dispersive objects," *Progress In Electromagnetics Research*, Vol. 96, 155–172, 2009.
15. Tang, M. and J. F. Mao, "Transient analysis of lossy nonuniform transmission lines using a time-step integration method," *Progress In Electromagnetics Research*, Vol. 69, 257–266, 2007.
16. Orlandi, A. and C. R. Paul, "FDTD analysis of lossy, multiconductor transmission lines terminated in arbitrary loads," *IEEE Trans. Electromagn. Compat.*, Vol. 38, No. 3, 388–399, Aug. 1996.